Nanoscale Advances

ROYAL SOCIETY OF CHEMISTRY

PAPER

View Article Online
View Journal | View Issue

Check for updates

Cite this: *Nanoscale Adv.*, 2020, **2**, 3858

Strong suppression of emission quenching in core quantum dots coupled to monolayer MoS_2†

H. L. Pradeepa, Aveek Bid and Jaydeep K. Basu *

Non-radiative processes like energy and charge transfer in 0D–2D semiconductor quantum dot (QD)-transition metal dichalcogenides (TMDs) and other two-dimensional layered materials, like graphene and analogs, leading to strong quenching of the photoluminescence (PL) of the usually highly emissive QDs, have been widely studied. Here we report control of the emission efficiency of core QDs placed in close proximity to the monolayers of MoS_2. The QDs are transferred in the form of a high-density compact monolayer with the dot–dot separation, δ as well as the MoS_2–QD separation, d, being controlled through chemical methods. While at larger separations we observe some quenching due to non-radiative processes, at smaller separations we observe enhanced emission from QDs on MoS_2 as compared to the reference despite the presence of significant non-radiative charge transfer. Interestingly, at small separations δ, we see evidence of strong dot–dot interactions and a significant red shift of QD PL which enhances spectral overlap with the B exciton of MoS_2. However, we observe significant reduction of PL quenching of QDs relative to longer δ and d cases, despite increased probability of non-radiative resonant energy transfer to MoS_2, due to the enhanced spectral overlap, as well as charge transfer. Significantly we observe that simultaneously the intensity of the B exciton of MoS_2 increases significantly suggesting the possibility of coherent and resonant radiative energy exchange between the 0D excitons in QDs and the 2D B exciton in MoS_2. Our study reveals interesting nanoscale light–matter interaction effects which can suppress quenching of QDs leading to potential applications of these nanoscale materials in light emitting and photonic devices.

Received 12th May 2020
Accepted 6th July 2020

DOI: 10.1039/d0na00384k

rsc.li/nanoscale-advances

Open Access Article. Published on 06 Julie 2020. Downloaded on 2025-11-29 9:53:09 nm..
This article is licensed under a Creative Commons Attribution-NonCommercial 3.0 Unported Licence.

1 Introduction

Hybrid devices consisting of monolayers of two-dimensional (2D) layered transition metal dichalcogenides (TMDs) like MoS_2 and zero-dimensional (0D) semiconductor quantum dots (QDs) have attracted increasing interest over the last decade.[1–5] From the fundamental perspective, interest has been focused on the novel aspects of light–matter interactions that can occur between the two nanoscale materials in the form of energy and charge transfer processes between photo excited excitons which can be generated in one or both the layers, while under certain conditions, formation of interlayer or hybrid excitons can also take place.[6–8] Thus these materials act as a playground for rich excitonic physics due to the interaction of 0D and 2D excitons with the 0D excitons being size tunable, while the 2D exciton being electrically and chemically tunable.[2,9,10] Apart from interest in the fundamental science of these systems, there has been tremendous interest in their potential applications in photo-detectors, photovoltaic devices, photocatalysts and sensors.[11–13] Most of the applications rely on the broad band gap tunability and highly efficient light harvesting properties of the QDs and the electrical properties, especially the high carrier mobility, of the TMDs which has led to development of various ultra-thin nanoscale opto-electronic devices[13–15] based on this hybrid architecture. A key aspect in such device applications is the ability to tune the rate of energy or charge transfer after photo-excitation of the QDs to the TMDs by spectral tuning of the QDs or through electrical or chemical control of carrier density and mobility of the TMDs. In all cases, the device application relies on fast energy or charge transfer from 0D excitons in the photo-excited QDs to the TMDs leading to strong quenching of the dots. As a result, these materials are not very useful as light emitting or photonic devices and it is not possible to utilize the ability to tune the brightness of these emitters (QDs) through electrical control of the TMD based field effect transistor (FET) devices.

Here we report control of the emission efficiency of core QDs placed in close proximity to the monolayers of MoS_2. The QDs are transferred in the form of a high-density compact monolayer with the dot–dot separation, δ as well as the MoS_2–QD separation, d, being controlled through chemical methods. At larger separations δ and d, we observe some quenching of QD emission on MoS_2 relative to emission

Department of Physics, Indian Institute of Science, Bangalore 560012, India. E-mail: basu@iisc.ac.in

† Electronic supplementary information (ESI) available: S1: CdSe QD synthesis; S2: MoS_2 PL fitting details, *etc.* See DOI: 10.1039/d0na00384k

This journal is © The Royal Society of Chemistry 2020

Open Access Article. Published on 06 Julie 2020. Downloaded on 2025-11-29 9:53:09 nm..
This article is licensed under a Creative Commons Attribution-NonCommercial 3.0 Unported Licence.

intensity on a silicon substrate, due to non-radiative processes. Surprisingly, at smaller separations we observe reduced quenching of QD emission on MoS_2, despite the presence of significant non-radiative charge transfer. Interestingly, at small separations δ, we see evidence of strong dot–dot interactions and a significant red shift of QD PL spectral maxima which enhances spectral overlap with the absorption of B excitons of MoS_2. However, instead of increased probability of non-radiative resonant energy transfer to MoS_2 from QDs and strong quenching of QD photoluminescence (PL), due to the enhanced spectral overlap, we find considerable reduction in the quenching of the PL of QDs compared to that expected from standard non-radiative processes. Significantly we observe that simultaneously the intensity of the B exciton of MoS_2 increases significantly suggesting the possibility of coherent and resonant radiative energy exchange between the 0D excitons in QDs and the 2D B exciton in MoS_2. Our study reveals interesting nanoscale light–matter interaction effects which can suppress the conventional quenching of QDs leading to potential applications of these nanoscale devices in light emitting and photonic devices.

2 Experimental details

MoS_2 monolayers were exfoliated on polydimethylsiloxane (PDMS) sheets and then transferred onto 300 nm SiO_2 substrates. Monolayers were confirmed through optical and Raman spectroscopy. QDs were synthesized following methods described earlier.[16,17] The monolayer of QDs was transferred onto MoS_2 using the Langmuir–Blodgett (LB) technique.[18,19] QDs in chloroform were spread on a deionized (DI) water-filled LB trough(Kibron Microtrough G2, Finland) to get a monolayer and the monolayer was slowly transferred onto the substrate at constant surface pressure. The ligand exchange was done by slightly modifying an earlier[20] report (ESI†). In a typical ligand exchange, the vapor of K_2S in formamide solution was exposed to the QD–MoS_2 sample overnight and the excess ligand was washed with toluene and formamide solution, and using this method we exchanged the TOPO (long) ligand with the sulfur (short) ligand.

Atomic force microscopy was performed using a Park system (NX model) in non-contact mode. PL spectra were collected using a Horiba (LabRam model) instrument, using a 532 nm continues wave (CW) laser. A laser power of $\sim$ 1 μW was used to avoid the bleaching of QDs. Signals were collected using a charge coupled device (CCD). A 300 g mm^{-1} grating and 1800 g mm^{-1} grating were used to collect the PL and the Raman spectra respectively. Time resolved PL (TRPL) data were collected using a PicoQuant MicroTime 200 system, with a temporal resolution of 25 ps. A 507 nm laser with 40 MHz repetition rate was used to excite the sample keeping the power at $\sim$ 1 μW. A band pass filter was used to collect QD TRPL spectra. A 50× (Olympus NA-0.45) objective was used to collect both PL and TRPL data.

3 Results and discussion

Fig. 1 shows the schematic of how the ligand exchange affects the separation (coupling) between the QD–MoS_2 hetero-structure. The ligand exchange not only decreases the separation d between the QDs and MoS_2 but also decreases the separation between the QDs δ themselves. When the long TOPO capped ligand is attached to QDs the d is $\sim$2 nm, and the δ is $\sim$4 nm. After ligand exchange these separations decrease to $\sim$0.3 nm and $\sim$0.6 nm respectively.

Fig. 2(a) shows the optical image of MoS_2 before the transfer of monolayer QDs. Fig. 2(b) shows the optical images of the MoS_2–QD hetero-structure after transferring the monolayer of the QD film using the LB technique. The QD monolayer is transferred uniformly onto the MoS_2 layer. Fig. 2(c) shows the isotherm (surface pressure *vs.* area plot) of LB transfer; the QD monolayer was transferred at a surface pressure of 35 mN m^{-1}. The 0D–2D hetero-structures were further characterized using atomic force microscopy (AFM). Fig. 2(d) shows the Raman spectra of MoS_2 and the MoS_2–QD hetero-structure before and after ligand exchange. The A_{1g} mode is slightly affected after transferring the QD layer.

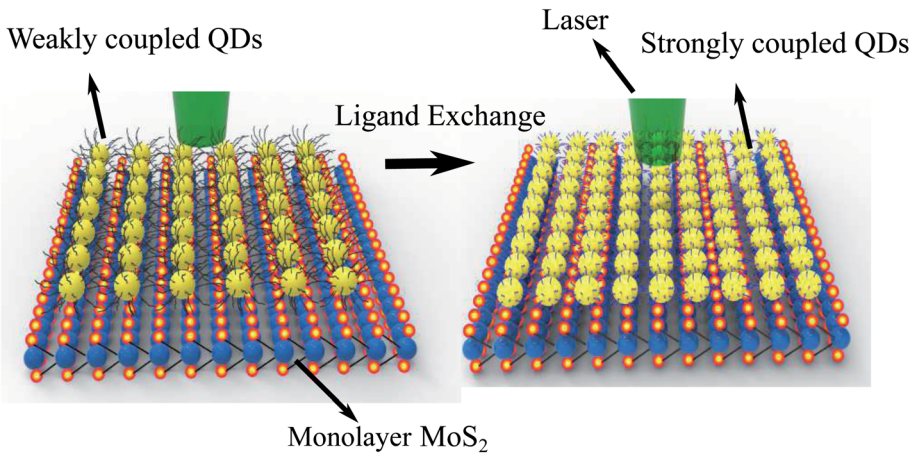

Fig. 1 The schematic of how the ligand exchange treatment affects the separation between the QD–MoS_2 hetero-structure; this treatment also modifies the dot–dot separation.

Open Access Article. Published on 06 Julie 2020. Downloaded on 2025-11-29 9:53:09 nm..
This article is licensed under a Creative Commons Attribution-NonCommercial 3.0 Unported Licence.

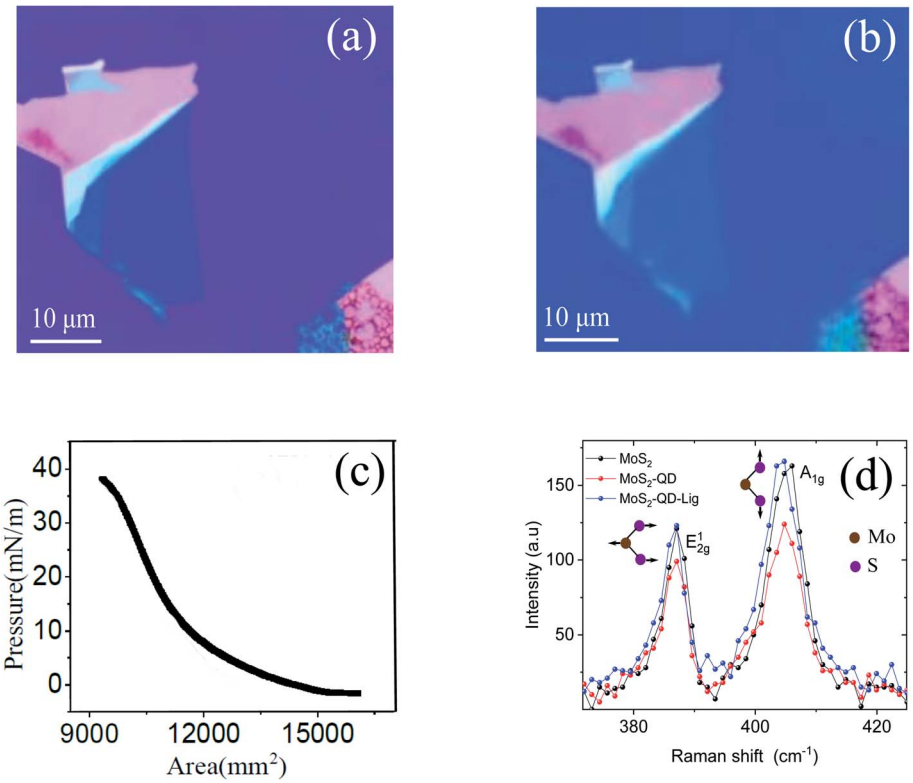

Fig. 2 (a) Optical image of monolayer MoS_2. (b) The optical images of the MoS_2–QD hetero-structure after transferring the compact monolayer of the QD film using the Langmuir–Blodgett (LB) technique, with the dot–dot separation, δ and the MoS_2–QD separation, d, being controlled through chemical methods. (c) The surface pressure *vs.* area (isotherm) curve of LB for the QD monolayer; the film was transferred at a surface pressure of 35 mN m^{-1}. (d) The Raman spectra of MoS_2, MoS_2–QDs, and MoS_2–QDs after ligand exchange.

Fig. 3 shows the PL spectra of the QD–MoS_2 hetero-structure. The energy of QDs was at 2.168 eV. The MoS_2 PL spectra consist of two excitonic peaks at ~1.85 eV and ~2 eV, related to spin–orbit splitting in the valence band.[21,22] The emission spectra of the chosen QD overlap with the absorption spectra of the higher energy exciton peak of MoS_2. Both the PL intensities of QDs and MoS_2 decrease in the hetero-structure compared to the PL intensity of the individuals on SiO_2, consistent with previous reports.[1,2] To quantify the quenching we introduce the quenching factor Q defined as $Q = I_{SiO_2}/I_{MoS_2}$, where I_{SiO_2} is the intensity of QDs on SiO_2, and I_{MoS_2} is the intensity of QDs on MoS_2. When d is ~2 nm, the value of Q is ~2.12 ± 0.05. Further the QD energy is blue shifted from 2.168 eV to 2.182 eV which is due to the coupling in the hetero-structure.[4] After ligand exchange, the distance between MoS_2 and QD reduces to ~0.3 nm, and the value of Q becomes 1.42 ± 0.01. It can be noted that the PL maxima significantly red shift to 2.091 eV and 2.069 eV on SiO_2 and MoS_2, respectively (Table 1). The full width

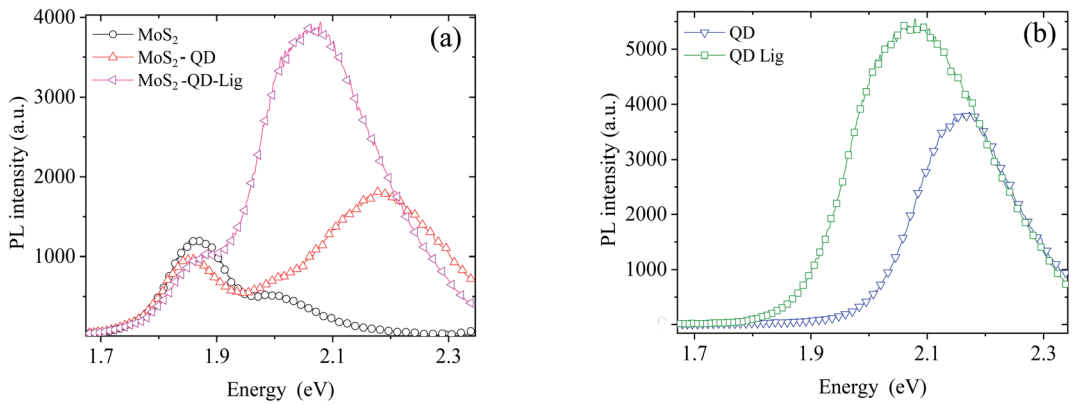

Fig. 3 PL data of (a) the QD–MoS_2 monolayer hetero-structure before and after ligand exchange while (b) shows the same on SiO_2 before and after ligand exchange.

 This journal is © The Royal Society of Chemistry 2020

Open Access Article. Published on 06 Julie 2020. Downloaded on 2025-11-29 9:53:09 nm..
This article is licensed under a Creative Commons Attribution-NonCommercial 3.0 Unported Licence.

Table 1 QD PL spectra fitting parameters like center, FWHM, and maxima corresponding to the data in Fig. 3. Detailed fitting is available in Section 3 of the ESI

System	Centre (eV)	FWHM (meV)	Intensity (a.u)
QD	2.168 ± 0.002	203 ± 6	3766 ± 17
QD-Lig	2.091 ± 0.004	263 ± 9	5501 ± 12
MoS_2–QD	2.182 ± 0.001	210 ± 4	1770 ± 36
MoS_2–QD-Lig	2.069 ± 0.004	218 ± 2	3847 ± 27

at half maximum (FWHM) of the QD monolayer on SiO_2 is increased from 203 meV to 263 meV after ligand exchange; this broadening and red shift indicate that the coupling between QDs in the highly compact itself has increased due to reduction in δ.[23–25] The details are shown in Table 1. Thus the analysis of PL spectra already reveals significant reduction in expected QD PL quenching. However, we do not have complete information about the energy or charge transfer processes from these PL spectra which are known to occur between these 0D–2D hybrid materials. For this we next discuss the TRPL data collected on the same systems as discussed above.

Fig. 4 shows the TRPL data of the QD in the QD–MoS_2 monolayer hetero-structure. All data can be fitted with bi-exponential functions. For the QD monolayer before ligand exchange on SiO_2 the longer lifetime (amplitude) τ_1 is 5.8 ns (30%), while the shorter lifetime (amplitude) τ_2 is 0.9 ns (70%) with the total weighted average lifetime τ of 4.5 ns. On MoS_2 these values become $\tau_1 = 4.4$ ns (17%), $\tau_2 = 0.7$ ns (83%), and $\tau = 2.8$ ns, respectively. This decrease in lifetime along with the decrease in PL intensity of QD PL on MoS_2 indicates non-radiative energy transfer from the QD monolayer to MoS_2. After ligand exchange and a consequent reduction of δ and d, τ on SiO_2 itself decreases to 1.4 ns with $\tau_1 = 3.0$ ns (10%), and $\tau_2 = 0.5$ ns (90%). This indicates that the coupling between QDs has significant influence on the lifetime. The lifetime further decreases on MoS_2 after ligand exchange to 0.9 ns with $\tau_1 = 2.6$ ns (5%), and $\tau_2 = 0.3$ ns (95%). This decrease indicates the enhanced nonradiative decay rate of the QD monolayer in the hetero-structure after the ligand exchange. Table 2 shows the lifetime details of QDs in the hetero-structure. The longer lifetime is usually associated with the intrinsic decay of the QDs while the shorter lifetime can be associated with the interaction between QDs or with the surrounding environment.[26–28] So the shorter lifetime and its amplitude will be very sensitive to the changes in the environment.

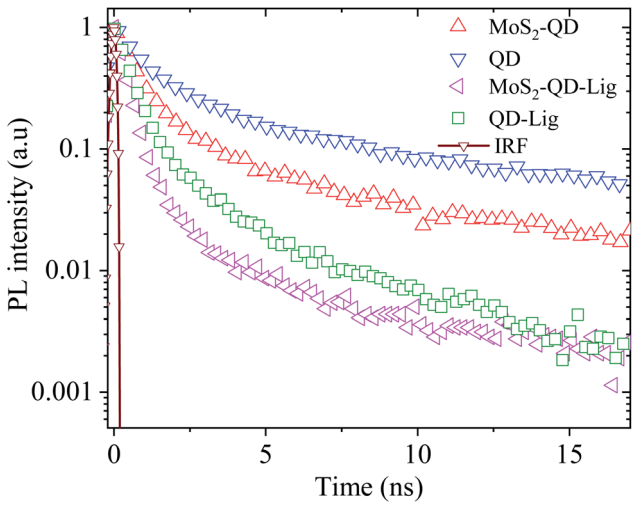

Fig. 4 TRPL data of the QD–MoS_2 monolayer hetero-structure along with the instrument response function (IRF). All data were fitted with bi-exponential functions as discussed in the ESI.†

Two major non-radiative processes have been suggested to occur in such 0D–2D hybrids[29] – Förster resonance energy transfer (FRET) and charge transfer (CT). The nonradiative energy transfer rate, Γ_{FRET}, for emitters on 2D materials like graphene and MoS_2, is related to the distance, d, as follows,[2,29]

$$\Gamma_{FRET} \sim \frac{1}{d^4}\int_0^\infty \alpha(E)g(E)E^4 dE: \quad (1)$$

where $\alpha(E)$ is the absorption profile of MoS_2, and $g(E)$ is the emission profile of the QDs. It is clear from eqn (1) that Γ_{FRET} is expected to increase significantly with decreasing d and hence a strong enhancement in Γ_{FRET} is expected in our systems after ligand exchange. Moreover, the broadening of the QD PL spectra along with significant red shift after ligand exchange could enhance the overlap with the MoS_2 absorption spectra. This is also expected to further enhance Γ_{FRET} in the ligand exchanged system leading to stronger emission quenching. However, this is not observed in our PL measurements as discussed earlier.

While there are several methods to estimate Γ_{FRET} we have utilized a method which combines information from both the PL and TRPL measurements following[2]

$$I_{QD} \sim \frac{\Gamma_r}{\Gamma_r + \Gamma_{nr}}. \quad (2)$$

$$I_{MoS_2-QD} \sim \frac{\Gamma_r}{\Gamma_r + \Gamma_{nr} + \Gamma_{FRET}}. \quad (3)$$

Table 2 The lifetime of QDs in different cases. τ is the total weighted average lifetime. Longer and shorter lifetimes are the extracted lifetimes with corresponding contributions in brackets using the bi-exponential fitting

System	Longer lifetime τ_1 (ns)	Shorter lifetime τ_2 (ns)	τ (ns)
QD	5.8 ± 0.04 (30 ± 2.0%)	0.9 ± 0.04 (70 ± 3.0%)	4.56 ± 0.05
QD-Lig	3.0 ± 0.04 (10 ± 1.0%)	0.5 ± 0.03 (90 ± 1.5%)	1.48 ± 0.01
MoS_2–QD	4.4 ± 0.05 (17 ± 1.6%)	0.7 ± 0.03 (83 ± 2.0%)	2.76 ± 0.07
MoS_2–QD-Lig	2.6 ± 0.05 (5 ± 0.5%)	0.3 ± 0.03 (95 ± 1.9%)	0.94 ± 0.11

Open Access Article. Published on 06 Julie 2020. Downloaded on 2025-11-29 9:53:09 nm..
This article is licensed under a Creative Commons Attribution-NonCommercial 3.0 Unported Licence.

From the above expressions and using $1/(\Gamma_r + \Gamma_{nr}) = \tau_{QD}$ we get

$$\Gamma_{FRET} = \frac{Q-1}{\tau_{QD}} \quad (4)$$

For the TOPO capped QD monolayers, using the value $Q = 2.12 \pm 0.05$ for longer capped QDs, from the above equation we get $\Gamma_{FRET} = (2.4 \pm 0.08) \times 10^8\ s^{-1}$. Similarly after ligand exchange, using the value $Q = 1.43 \pm 0.01$ we get $\Gamma_{FRET} = (2.8 \pm 0.04) \times 10^8\ s^{-1}$.

This slight increase in Γ_{FRET} is due to the decrease in d and the increase in the spectral overlap after ligand exchange. But, as discussed in eqn (1), Γ_{FRET} varies, as $1/d^4$ according to eqn (1). The center to center distance is calculated from the AFM data (see ESI Fig. S7†) of the QD film by taking the radius of QDs which is $\sim$ 3.5 nm before ligand exchange and $\sim$2 nm after ligand exchange with half the MoS_2 thickness (0.3 nm) being added to these values. The ratio of $1/d^4$ after and before ligand exchange is $\sim$7.4. Also the increase in the spectral overlap should further increase the FRET rate in the system. However the ratio of Γ_{FRET} after and before ligand exchange is only $\sim$1.1, which suggests that FRET is not the dominant energy transfer process in our hetero-structures. This is surprising given the spectral overlap.

It is well known that there are several conditions which need to be satisfied for FRET to take place between emitters and 2D semiconductors. Two of the main factors are spectral overlap (absorption of MoS_2 and emission of QDs) and small separation. However, another key factor is related to the kinetics of energy transfer. This involves comparison of the lifetime, τ, of the QD and $(\Gamma_{FRET})^{-1}$. Basically, $\tau > (\Gamma_{FRET})^{-1}$ for FRET to be dominant. It is to be noted that τ, for our case, has two components, τ_1 and τ_2 (Table 2). As mentioned earlier, the longer lifetime, τ_1, is the intrinsic excitonic decay while the shorter one, τ_2, is due to the QD–QD interaction which is dominant in our compact QD monolayer films. In fact, even for pristine QD films the weight factor for τ_2 is $\sim$70% and this becomes even more dominant upon adding additional decay channels due to interactions with MoS_2 or even upon ligand exchange on SiO_2 leading to much shorter QD–QD lateral separation and hence even stronger interactions. Clearly, in our compact QD monolayer films τ (τ_2) < $(\Gamma_{FRET})^{-1}$. While this relationship might also hold for τ_1 it is definitely valid for τ_2, which, in any case, is the dominant lifetime component. This suggests that there are alternative processes which lead to enhancement of decay rate.

However, since our QDs are core only it is possible that other non-radiative processes can exist, especially charge transfer (CT), as has been also suggested to occur in these systems.[11,30,31] Some indication of the presence of CT is also revealed from analysis of the PL data of MoS_2. For example, if we consider the ratio $I_{trion}/I_{exciton}$ for MoS_2 with the TOPO capped QD monolayer on top we find it to be 1.18. We observe an increase in this ratio from 1.18 to 2.08 after ligand exchange treatment of QDs on MoS_2 suggesting an increase in CT. However, we did not observe a significant change in the MoS_2 PL intensity suggesting that other, possibly, radiative processes might be in operation in the hetero-structures. Nevertheless, if we consider that the CT is present, the CT rate can be estimated using the expression:[11]

$$\Gamma_{CT} = \frac{1}{\tau_{MoS_2-QD}} - \frac{1}{\tau_{QD}}, \quad (5)$$

where Γ_{CT} is the CT rate, τ_{MoS_2-QD} is the total average lifetime of QDs on MoS_2, and τ_{QD} is the total average lifetime of QDs on SiO_2. We find that before ligand exchange this rate is $(1.4 \pm 0.2) \times 10^8\ s^{-1}$ while after ligand exchange this increases to $(3.9 \pm 0.07) \times 10^8\ s^{-1}$. These values are also consistent with enhanced CT in our system after ligand exchange as predicted by the Marcus theory. Conventionally the charge transfer rate increases exponentially with decreasing the distance. The ratio of CT after and before ligand exchange is expected to be ${e_2}^{-d}/{e_1}^{-d} = 4.51$, however this ratio from the calculated CT rates is 2.7, suggesting that the CT rate might not be following the Marcus theory. However, we now consider the shorter lifetime component, τ_2, to compare the CT rates since it is the dominant time scale of relaxation of PL and is also most sensitive to the QD interactions with its environment as discussed earlier. The calculated CT rate from the above expression for τ_2 is $(3.2 \pm 0.1) \times 10^8\ s^{-1}$ and $(1.3 \pm 0.2) \times 10^9\ s^{-1}$ before and after ligand exchange respectively. The ratio of CT rates after and before ligand exchange turns out to be 4.16, which is close to ${e_2}^{-d}/{e_1}^{-d}$. This suggests that the CT process is the dominant non-radiative process (and not FRET) in our hybrid structures and the d dependence of Γ_{CT} is reasonably consistent with the exponential d dependence predicted by the Marcus theory, as seen earlier.[11] However, this does not explain the observed reduction in PL quenching of QDs after ligand exchange on MoS_2.

We now consider the effect of resonant radiative energy transfer from the QD to MoS_2 due to the spectral overlap between the QD and B exciton. In order to understand this possible mechanism better we carefully fitted the PL spectra with the combination of Lorentzian and Gaussian peak functions. It is to be noted that (ESI Fig. S2†) pure MoS_2 PL spectra can be well modeled with 3 Lorentzians corresponding to the A exciton and trion and B exciton. On the other hand the QD PL on SiO_2 which shows extrinsic broadening due to size dispersity and thermal effects can be well fitted with a single Gaussian peak fitting function (ESI Fig. S3†). Fig. 5(a) shows the cumulative fit of the full PL spectrum including that of MoS_2 and QDs and also displays the individual fits to the A trion, exciton and B exciton components as well as that due to the QD peak for the TOPO capped QDs on MoS_2, using 3 Lorentzians (MoS_2)and 1 Gaussian (QD). It can be seen clearly that the intensity of the trion component is higher than that of A and B exciton components. Fig. 5(b) on the other hand shows the same fitted components, as in Fig. 5(a), corresponding to the system after ligand exchange. However, we could only fit the MoS_2–QD spectra satisfactorily with two Lorentzians (A exciton and trion) and two Gaussians (B exciton and QD). It is clearly observed that the B exciton intensity has increased compared to the other components on the A exciton as well as the QDs. The $I_{A\ exciton}/I_{B\ exciton}$ is decreased from 3.23 to 1.24 after transferring QDs onto MoS_2. This suggests that there is energy transfer between the

 This journal is © The Royal Society of Chemistry 2020

Open Access Article. Published on 06 Julie 2020. Downloaded on 2025-11-29 9:53:09 nm..
This article is licensed under a Creative Commons Attribution-NonCommercial 3.0 Unported Licence.

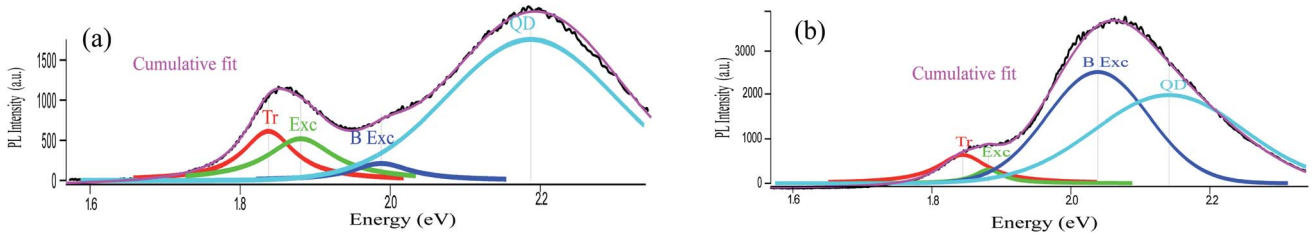

Fig. 5 PL data fitting for the QD–MoS_2 monolayer hetero-structure before and after ligand exchange: (a) fitting before ligand exchange shows that the intensity of B excitons is lower than that of the QD, A exciton and trion. (b) After ligand exchange the fit shows that the intensity of B excitons is higher than that of the QD, A trion and exciton.

QD and B exciton although we do not observe a similar decrease in QD PL intensity. In fact the QD component of the PL spectrum cannot be well fitted with a single Gaussian (ESI Fig. S4†) as well indicating a strong overlap between the B exciton (2D) and the QD exciton (0D). Thus coupled with the observation that after ligand exchange the PL spectra can be fitted better with 2 Lorentzians (MoS_2 A) and 2 Gaussians (QD + B), it is suggested that a hybrid state (0D–2D) in this resonantly coupled system is, possibly, formed with the B exciton and coupled QDs exchanging energy coherently such that simultaneous enhancement of B exciton intensity and strong suppression of QD PL quenching take place.

4 Conclusions

In summary, we control the emission efficiency of core QDs in the monolayers of the MoS_2–QD hetero-structure using ligand exchange treatment. At larger separations we observe quenching of QD PL due to non-radiative processes, at smaller separations we observe enhanced emission from QDs on MoS_2 as compared to the larger d despite the presence of significant non-radiative charge transfer. Interestingly, at small separations, we see evidence of strong dot–dot interactions and a significant red shift of QD PL maxima which enhances spectral overlap with the absorption of B excitons of MoS_2. Despite the increased probability of non-radiative resonant energy transfer to MoS_2 from QDs due to increased spectral overlap as well as that due to enhanced CT we find that the quenching of the PL of QDs is significantly reduced as compared to longer separations as well as to what would be expected from the non-radiative processes. Concurrent with this reduced QD PL quenching, the intensity of the B exciton of MoS_2 increases significantly suggesting the possibility of coherent and resonant radiative energy exchange between the 0D excitons in QDs and the 2D B exciton in MoS_2. We observe that the ligand exchange is an effective technique to tune the nonradiative decay channels in the 0D–2D hetero-structure. Our study reveals interesting nanoscale light–matter interaction effects which can suppress the conventional quenching of QDs leading to potential applications of these nanoscale devices in photonics.

Conflicts of interest

There are no conflicts to declare.

Acknowledgements

HLP thanks CSIR-UGC for financial support. The authors thank DST nanomission for funding. The authors thank SERB, India for funding. HLP thanks Mangesh and Puspender for help in using Igor software.

Notes and references

1 A. Raja, A. Montoya-Castillo, J. Zultak, X.-X. Zhang, Z. Ye, C. Roquelet, D. A. Chenet, A. M. Van Der Zande, P. Huang, S. Jockusch and T. F. Heinz, *Nano Lett.*, 2016, **16**, 2328–2333.
2 D. Prasai, A. R. Klots, A. Newaz, J. S. Niezgoda, N. J. Orfield, C. A. Escobar, A. Wynn, A. Efimov, G. K. Jennings and S. J. Rosenthal, *Nano Lett.*, 2015, **15**, 4374–4380.
3 H. Zang, P. K. Routh, Y. Huang, J.-S. Chen, E. Sutter, P. Sutter and M. Cotlet, *ACS Nano*, 2016, **10**, 4790–4796.
4 K. M. Goodfellow, C. Chakraborty, K. Sowers, P. Waduge, M. Wanunu, T. Krauss, K. Driscoll and A. N. Vamivakas, *Appl. Phys. Lett.*, 2016, **108**, 021101.
5 S. Sampat, T. Guo, K. Zhang, J. A. Robinson, Y. Ghosh, K. P. Acharya, H. Htoon, J. A. Hollingsworth, Y. N. Gartstein and A. V. Malko, *ACS Photonics*, 2016, **3**, 708–715.
6 A. Boulesbaa, K. Wang, M. Mahjouri-Samani, M. Tian, A. A. Puretzky, I. Ivanov, C. M. Rouleau, K. Xiao, B. G. Sumpter and D. B. Geohegan, *J. Am. Chem. Soc.*, 2016, **138**, 14713–14719.
7 P. Rivera, J. R. Schaibley, A. M. Jones, J. S. Ross, S. Wu, G. Aivazian, P. Klement, K. Seyler, G. Clark and N. J. Ghimire, *Nat. Commun.*, 2015, **6**, 1–6.
8 M. Okada, A. Kutana, Y. Kureishi, Y. Kobayashi, Y. Saito, T. Saito, K. Watanabe, T. Taniguchi, S. Gupta and Y. Miyata, *ACS Nano*, 2018, **12**, 2498–2505.
9 H. L. Pradeepa, P. Mondal, A. Bid and J. K. Basu, *ACS Appl. Nano Mater.*, 2020, **3**, 641–647.
10 J. S. Ross, S. Wu, H. Yu, N. J. Ghimire, A. M. Jones, G. Aivazian, J. Yan, D. G. Mandrus, D. Xiao and W. Yao, *Nat. Commun.*, 2013, **4**, 1474.
11 J.-S. Chen, M. Li, Q. Wu, E. Fron, X. Tong and M. Cotlet, *ACS Nano*, 2019, **13**, 8461–8468.
12 S. Zhang, X. Wang, Y. Chen, G. Wu, Y. Tang, L. Zhu, H. Wang, W. Jiang, L. Sun and T. Lin, *ACS Appl. Mater. Interfaces*, 2019, **11**(26), 23667–23672.

Open Access Article. Published on 06 Julie 2020. Downloaded on 2025-11-29 9:53:09 nm..
This article is licensed under a Creative Commons Attribution-NonCommercial 3.0 Unported Licence.

13 M. Li, J.-S. Chen, P. K. Routh, P. Zahl, C.-Y. Nam and M. Cotlet, *Adv. Funct. Mater.*, 2018, **28**, 1707558.
14 D. Kufer, I. Nikitskiy, T. Lasanta, G. Navickaite, F. H. Koppens and G. Konstantatos, *Adv. Mater.*, 2015, **27**, 176–180.
15 H. Chen, H. Liu, Z. Zhang, K. Hu and X. Fang, *Adv. Mater.*, 2016, **28**, 403–433.
16 L. Qu and X. Peng, *J. Am. Chem. Soc.*, 2002, **124**, 2049–2055.
17 C. de Mello Donega, S. G. Hickey, S. F. Wuister, D. Vanmaekelbergh and A. Meijerink, *J. Phys. Chem. B*, 2003, **107**, 489–496.
18 J. R. Heath, C. M. Knobler and D. V. Leff, *J. Phys. Chem. B*, 1997, **101**, 189–197.
19 M. Haridas, J. K. Basu, A. Tiwari and M. Venkatapathi, *J. Appl. Phys.*, 2013, **114**, 064305.
20 H. J. Yun, T. Paik, M. E. Edley, J. B. Baxter and C. B. Murray, *ACS Appl. Mater. Interfaces*, 2014, **6**, 3721–3728.
21 A. Kormányos, G. Burkard, M. Gmitra, J. Fabian, V. Zólyomi, N. D. Drummond and V. Fal'ko, *2D Mater.*, 2015, **2**, 022001.
22 K. F. Mak, K. He, C. Lee, G. H. Lee, J. Hone, T. F. Heinz and J. Shan, *Nat. Mater.*, 2013, **12**, 207.
23 J.-H. Choi, A. T. Fafarman, S. J. Oh, D.-K. Ko, D. K. Kim, B. T. Diroll, S. Muramoto, J. G. Gillen, C. B. Murray and C. R. Kagan, *Nano Lett.*, 2012, **12**, 2631–2638.
24 C. R. Kagan and C. B. Murray, *Nat. Nanotechnol.*, 2015, **10**, 1013.
25 J.-S. Lee, M. V. Kovalenko, J. Huang, D. S. Chung and D. V. Talapin, *Nat. Nanotechnol.*, 2011, **6**, 348.
26 W.-S. Chae, T. D. T. Ung and Q. L. Nguyen, *Adv. Nat. Sci.: Nanosci. Nanotechnol.*, 2013, **4**, 045009.
27 M. Praveena, T. Phanindra Sai, R. Dutta, A. Ghosh and J. K. Basu, *ACS Photonics*, 2017, **4**, 1967–1973.
28 R. Dutta, K. Jain, M. Venkatapathi and J. K. Basu, *Phys. Rev. B*, 2019, **100**, 155413.
29 B. Guzelturk and H. V. Demir, *Adv. Funct. Mater.*, 2016, **26**, 8158–8177.
30 H. Wu, Z. Kang, Z. Zhang, Z. Zhang, H. Si, Q. Liao, S. Zhang, J. Wu, X. Zhang and Y. Zhang, *Adv. Funct. Mater.*, 2018, **28**, 1802015.
31 A. J. Goodman, N. S. Dahod and W. A. Tisdale, *J. Phys. Chem. Lett.*, 2018, **9**, 4227–4232.

 This journal is © The Royal Society of Chemistry 2020